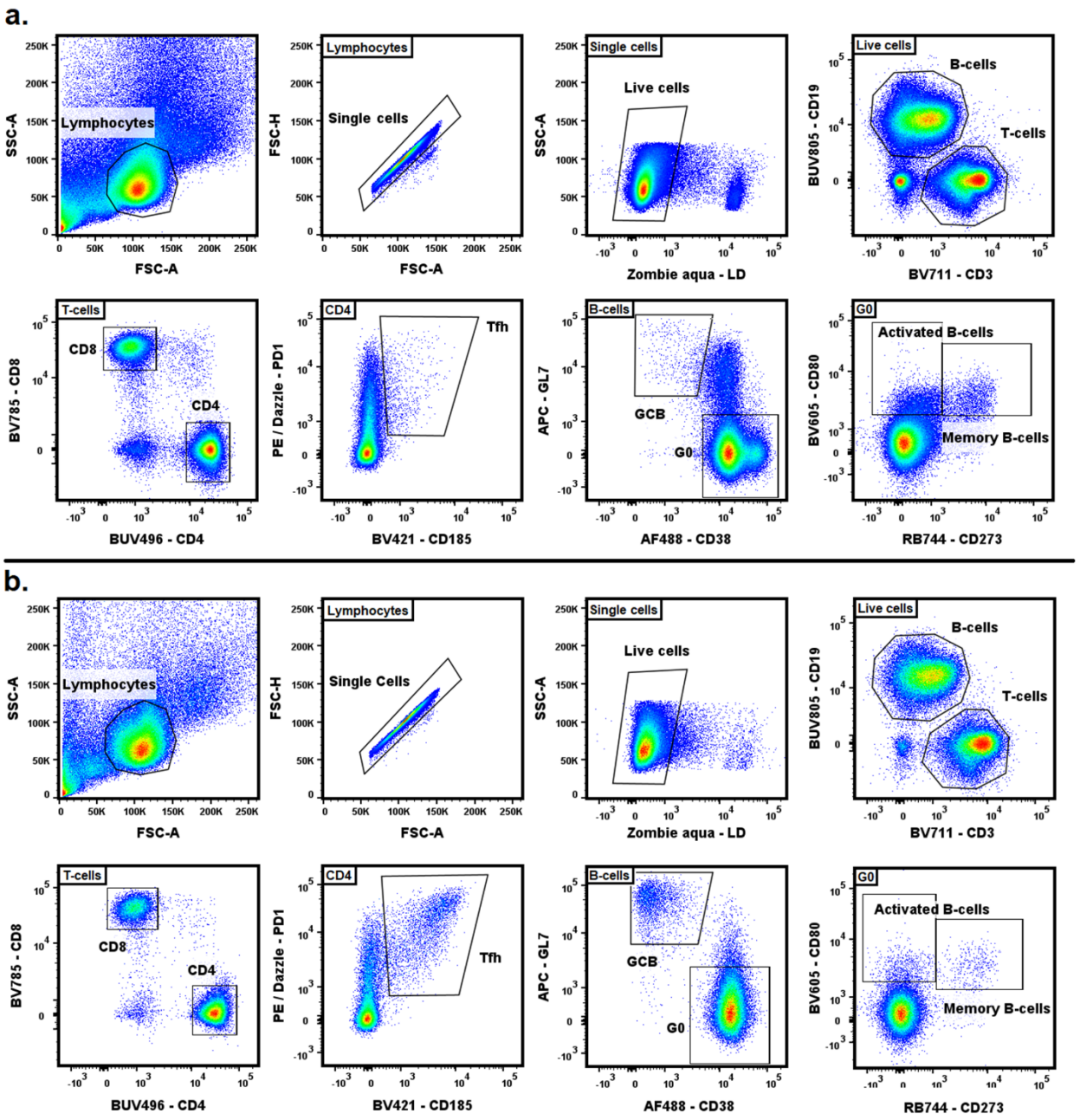

Supplementary Figure 1. Gating strategy for identifying Tfh, GCB, activated, and memory B-cells. a. Live B cells ($CD19^+$) and T cells ($CD3^+$) were gated following the exclusion of doublets, debris (based on FSC-A vs. SSC-A and FSC-A vs. FSC-H scatter plots), and dead cells (Zombie $Aqua^+$). Within T cells, follicular helper T (Tfh) cells were identified as $CD4^+PD1^+CD185^+$. Germinal center B (GCB) cells were defined as $CD19^+CD38^-GL7^+$. Activated and memory B cells were distinguished based on the expression of CD273 on $CD19^+CD38^+CD80^+$ cells. **b.** Cell phenotyping in NALT. The gating strategy applied was identical to that described above.

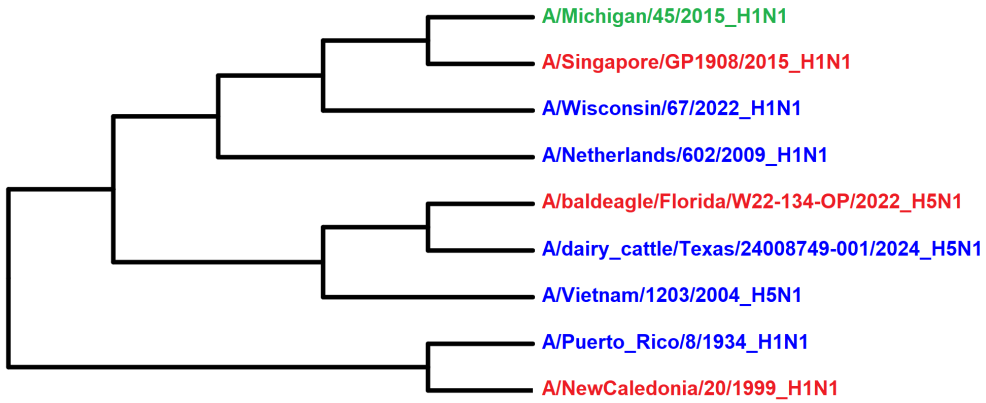

Supplementary Figure 2. A cladogram based on the amino acid sequence alignment of the NA proteins. Strains used in this study are highlighted in green (vaccine strain A/Michigan /45/2015 H1N1), red (used for challenge and serology analysis), and blue (used for serology analysis).

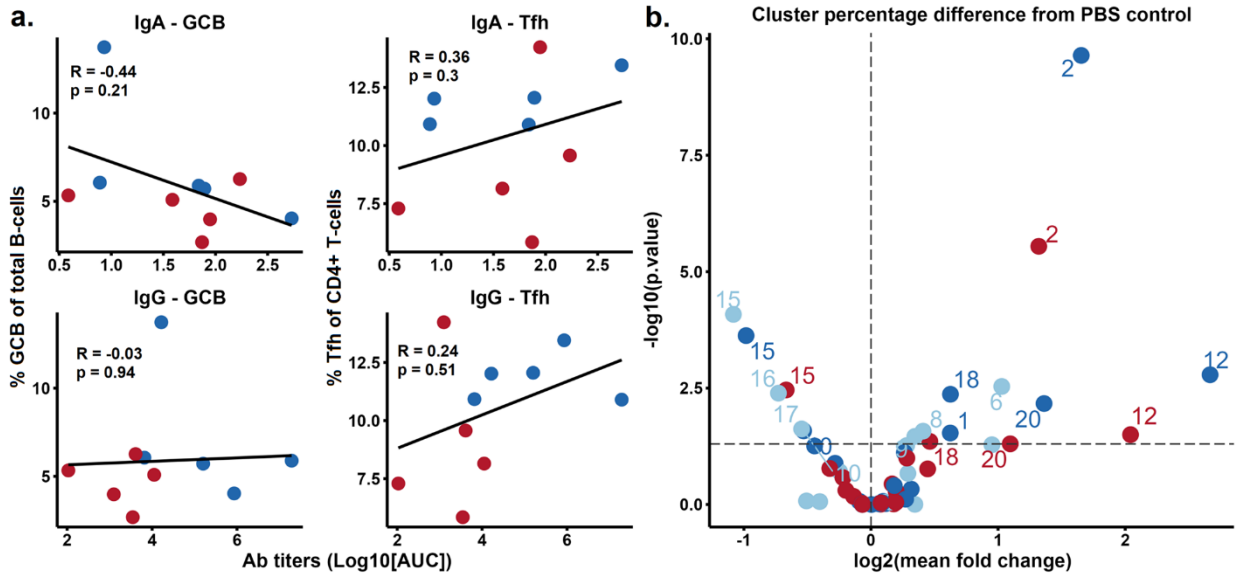

Supplementary Figure 3. a. Pearson's correlation between the percentage of Tfh and GCB in NALT and the mucosal IgA/IgG levels in nasal washes. **b**. Volcano plot representing the magnitude and significance of PhenoGraph cluster percentage changes compared to the corresponding values in the PBS-control group.

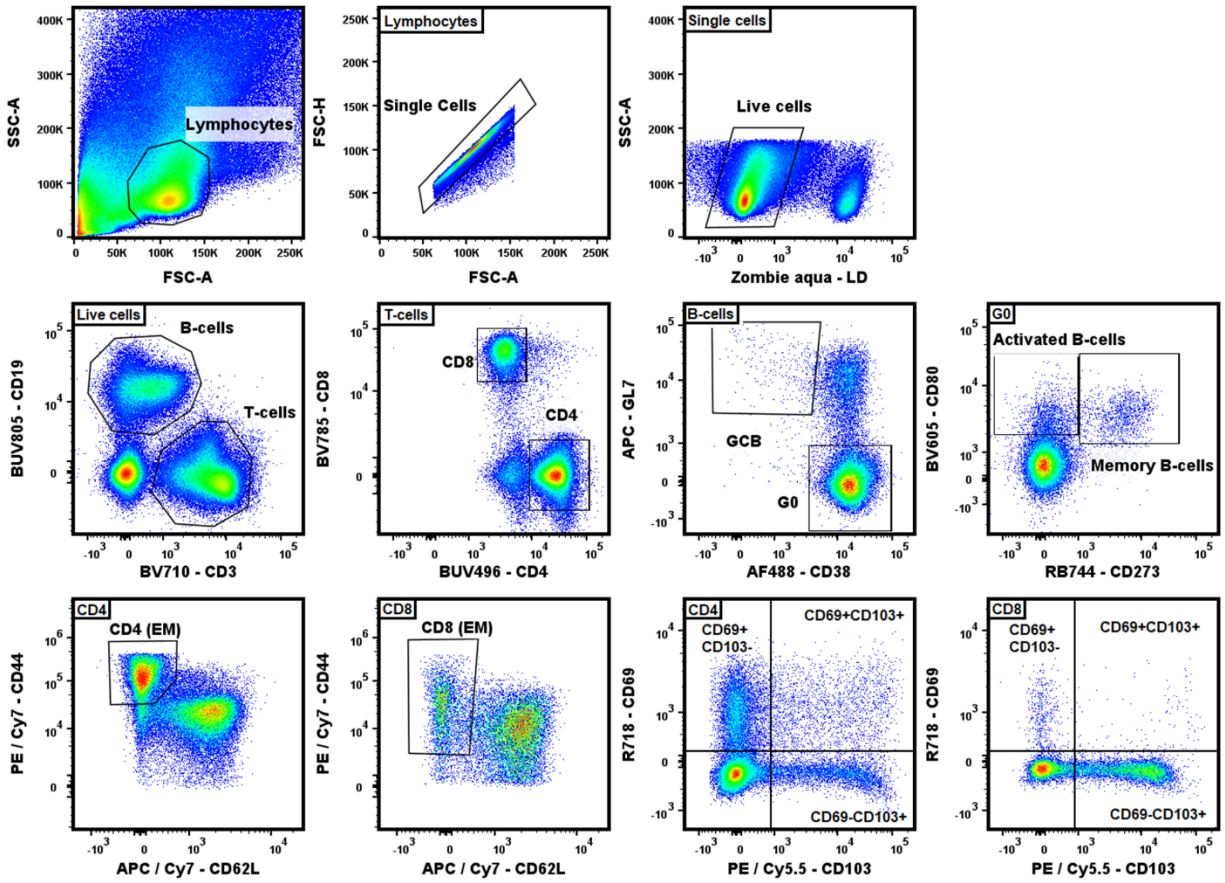

Supplementary Figure 4. Gating strategy for identifying B- and T-cell subpopulations in lungs. Live B cells ($CD19^+$) and T cells ($CD3^+$) were gated following the exclusion of doublets, debris (based on FSC-A vs. SSC-A and FSC-A vs. FSC-H scatter plots), and dead cells (Zombie $Aqua^+$). T cells were subdivided into $CD8^+$ and $CD4^+$ subpopulations; within the $CD4^+$ T-cells, follicular helper T (Tfh) cells were identified as $CD4^+PD1^+CD185^+$. EM cells within $CD8^+$ and $CD4^+$ subpopulations were identified as $CD62L^-CD44^+$. A combination of CD69 and CD103 markers was used to identify activated ($CD69^+$) and Trm ($CD103^+CD69^+$) cells. Germinal center B (GCB) cells were defined as $CD19^+CD38^-GL7^+$. Activated and memory B cells were distinguished based on the expression of CD273 on $CD19^+CD38^+CD80^+$ cells.

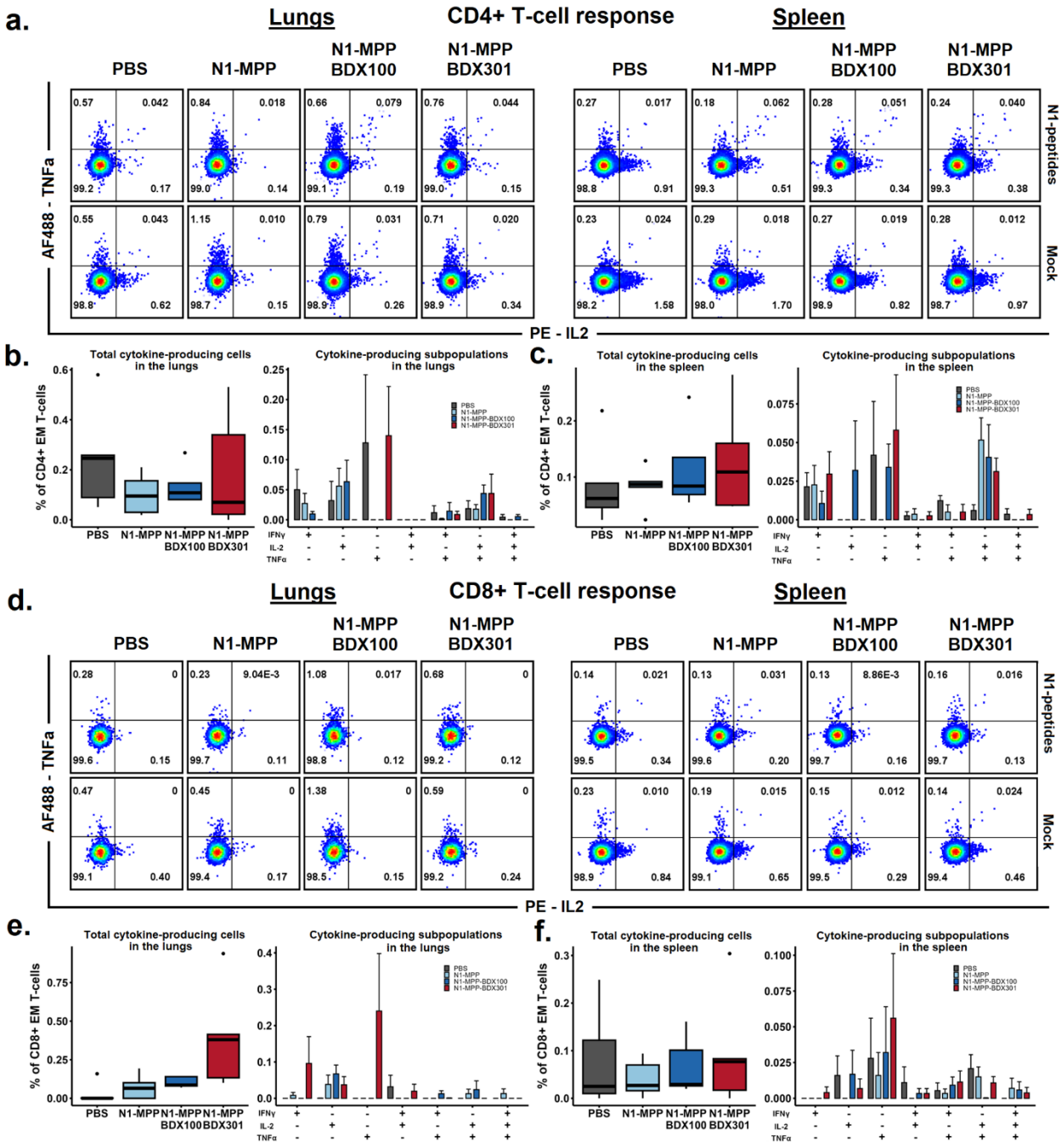

Supplementary Figure 5. T-cellular immune response to the rNA-N1-MPP vaccine adjuvanted with BDX100 or BDX301 in BALB/c mice. a., d. Flow cytometry plots showing the percentage of IL-2- and TNFα-producing $CD4^+$ and $CD8^+$ EM T-lymphocytes in mouse lungs and spleens 10 days after the booster immunization (gated on live $CD3^+CD19^-CD4/CD8^+CD62L^-CD44^+$ cells). Cells were incubated with overlapping peptides, covering the whole sequence of N1 NA-protein for 6h in the presence of Brefeldin A and co-stimulatory anti-CD28 antibodies. Plots

were produced by combining data from each separate sample into one file for each group. **b., c.** Percentage of different cytokine-producing cell populations within the total $CD4^+$ EM T-cell subset after background subtraction in the lungs (**b.**) and spleen (**c.**). **e., f.** Percentage of different cytokine-producing cell populations within the total $CD8^+$ EM T-cell subset after background subtraction in the lungs (**e.**) and spleen (**f.**). Average and SE values are shown.

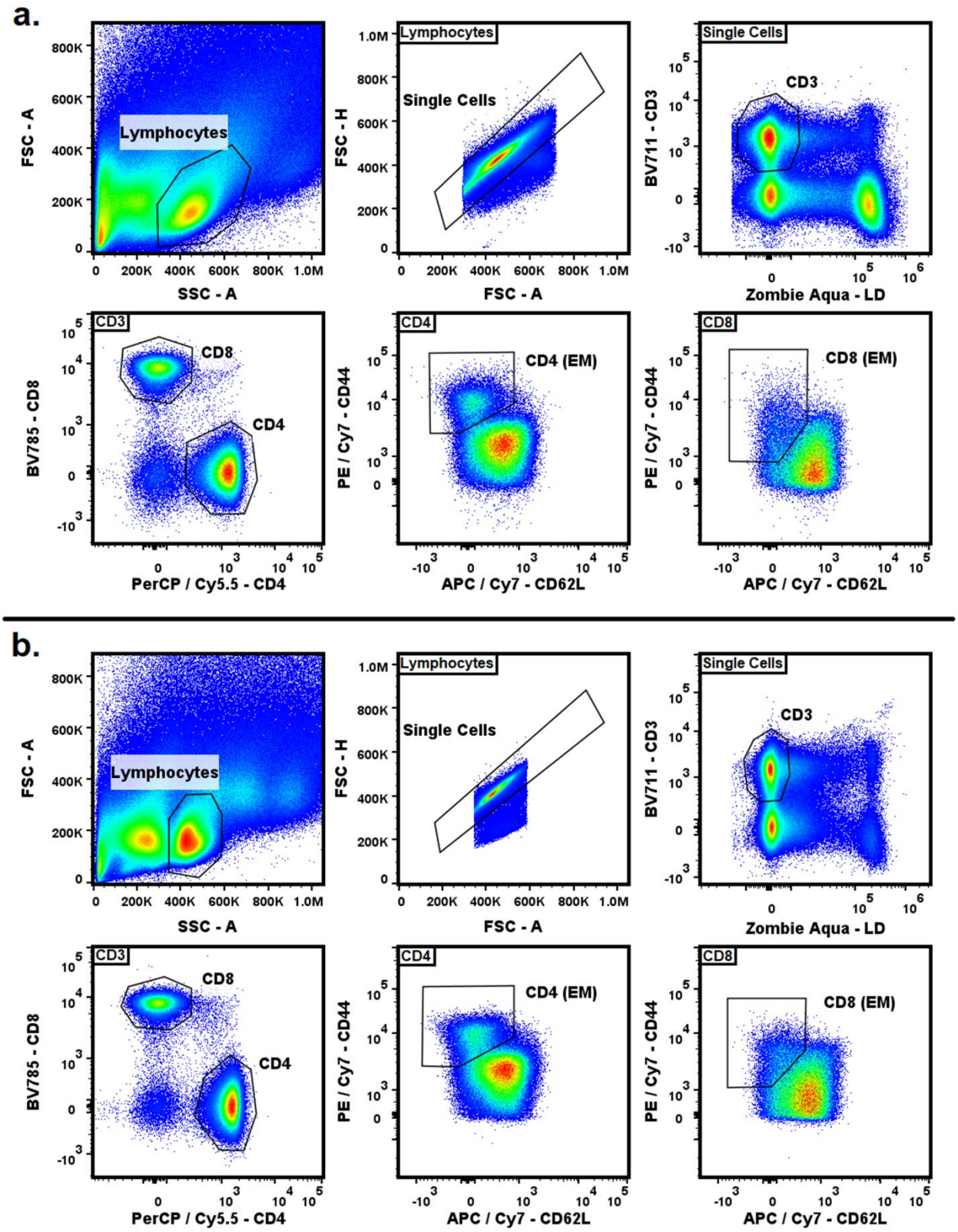

Supplementary Figure 6. Gating strategy for the identification of EM subpopulations in CD4$^+$ and CD8$^+$ T-cells. a. Gating strategy for lungs. Live T cells (CD3$^+$Zombie Aqua$^-$) were

gated following the exclusion of doublets and debris (based on FSC-A vs. SSC-A and FSC-A vs. FSC-H scatter plots). T cells were subdivided into $CD8^+$ and $CD4^+$ subpopulations. EM cells were identified as $CD62L^-CD44^+$. **b.** Gating strategy for spleen. The gating strategy applied was identical to that described above.

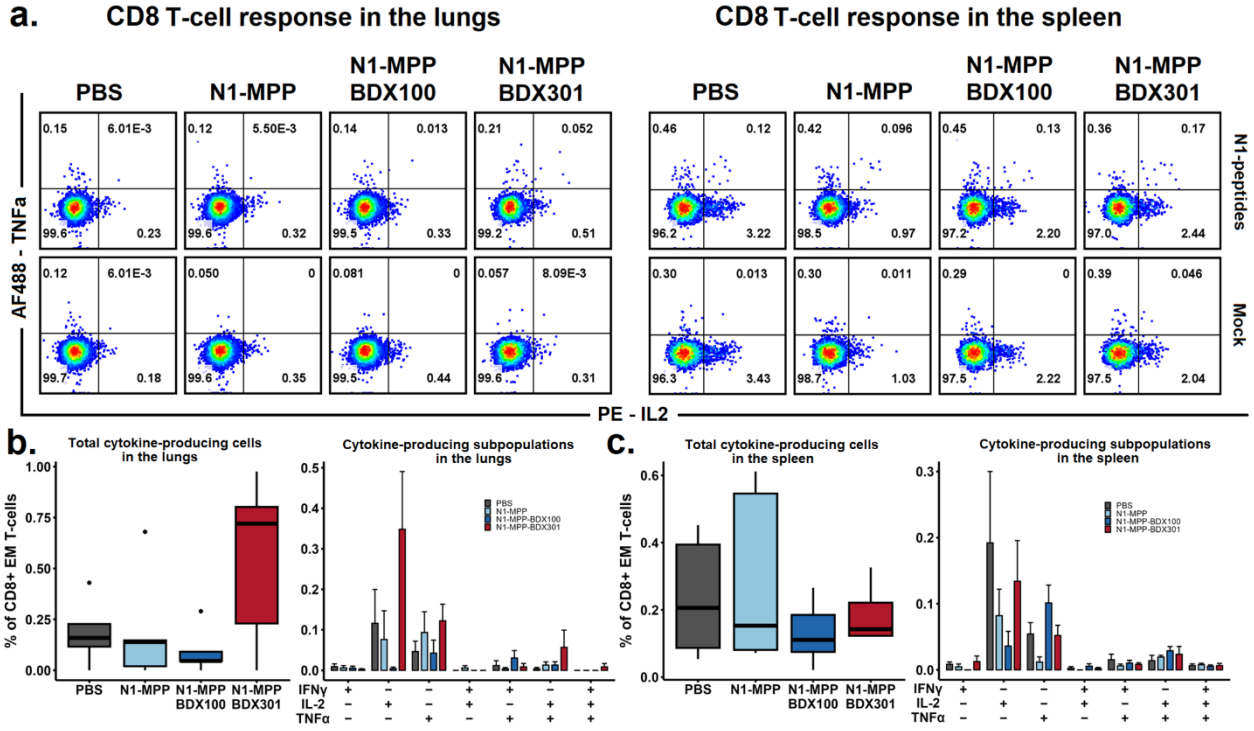

Supplementary Figure 7. $CD8^+$ T-cellular immune response to the N1-MPP vaccine adjuvanted with BDX100 or BDX301 in C57/Black-6 mice. a. Flow cytometry plots showing the combined data on the percentage of IL-2- and TNFα-producing $CD8^+$ EM T-lymphocytes in mouse lungs and spleens 10 days after the booster immunization. Cells were incubated with overlapping peptides, covering the whole sequence of N1 NA-protein for 6h in the presence of Brefeldin A and co-stimulatory anti-CD28 antibodies. Plots were produced by combining data from each separate sample into one file for each group. **b., c.** Percentage of different cytokine-producing cell populations within the total $CD8^+$ EM T-cell subset after background subtraction in the lungs (**b.**) and spleen (**c.**). Average and SE values are shown.

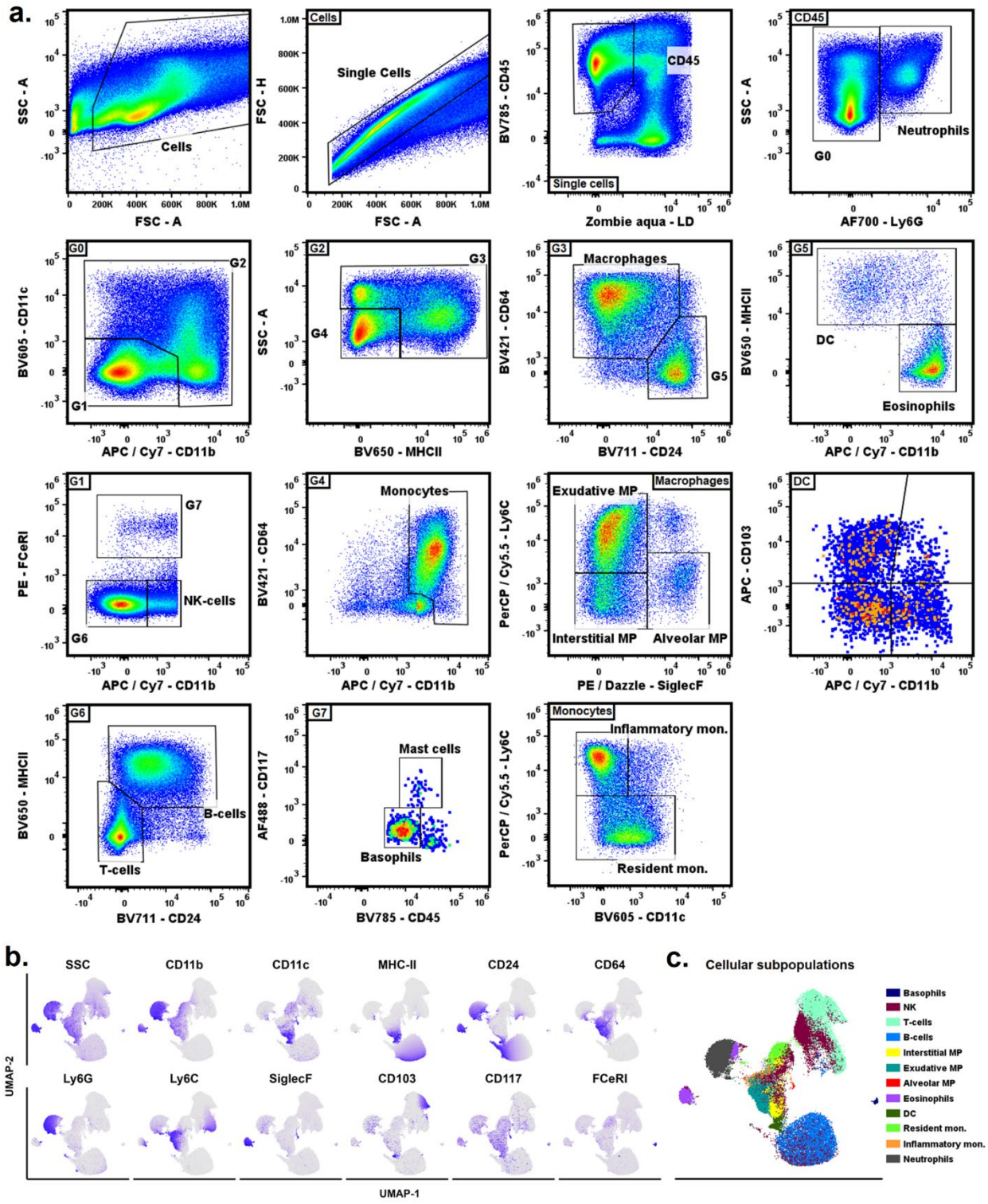

Supplementary Figure 8. a. Gating strategy for the identification of major cell populations in mouse lungs. Live CD45^{+} cells were isolated after the exclusion of doublets, debris (based on the FSC-A/SSC-A and FSC-A/FSC-H light scattering), and dead cells (Zombie Aqua^{+}). Gates

containing multiple cell populations are numbered (G1-G7). Gates containing a single cell population are labeled with the corresponding cell type. The panels allows to identify resident and inflammatory monocytes, interstitial (IMP), alveolar (AMP), and exudative macrophages (ExMP), neutrophils, eosinophils, basophils, mast cells, dendritic cells ($CD11b^{-}CD103^{-}$ (DC1), $CD11b^{-}CD103^{+}$ (DC2), $CD11b^{+}CD103^{-}$ (DC3), $CD11b^{+}CD103^{+}$ (DC4)), NK-cells, B-cells and T-cells. **b.** UMAP projections showing the differential expression of innate immune cells phenotype markers on lung cells. **c.** UMAP projection showing different innate immune cell subpopulations.